Gold Clusters

DOI: 10.1002/anie.201410295

The Structure and Optical Properties of the $[Au_{18}(SR)_{14}]$ Nanocluster**

Shuang Chen, Shuxin Wang, Juan Zhong, Yongbo Song, Jun Zhang, Hongting Sheng, Yong Pei, and Manzhou Zhu**

Abstract: *Decreasing the core size is one of the best ways to study the evolution from Au^I complexes into Au nanoclusters. Toward this goal, we successfully synthesized the $[Au_{18}(SC_6H_{11})_{14}]$ nanocluster using the $[Au_{18}(SG)_{14}]$ (SG = L-glutathione) nanocluster as the starting material to react with cyclohexylthiol, and determined the X-ray structure of the cyclohexylthiol-protected $[Au_{18}(C_6H_{11}S)_{14}]$ nanocluster. The $[Au_{18}(SR)_{14}]$ cluster has a Au_9 bi-octahedral kernel (or inner core). This Au_9 inner core is built by two octahedral Au_6 cores sharing one triangular face. One transitional gold atom is found in the Au_9 core, which can also be considered as part of the $Au_4(SR)_5$ staple motif. These findings offer new insight in terms of understanding the evolution from $[Au^I(SR)]$ complexes into Au nanoclusters.*

Metal nanoclusters of atomic precision have attracted great attention because of their use in catalysis, chemical sensing, or bio-application.[1–5] Unlike metal complexes (of e.g. Au^I, Ag^I) and larger metal nanoparticles, the atomic packing mode, and electronic structure in small nanoclusters play a much more important role in their structure–property relationship and size-dependent properties.[6] In the previous work, metal nanoclusters with small electronic structures (e.g. 2 or 4 free electrons) were reported.[7] These nanoclusters were considered as the bridge in linking metal complexes with metal nanoclusters. In the past few decades, thiolate-protected gold nanoclusters have attracted interest and during the past eight years the structures of clusters of Au_{102},[8] Au_{38},[9] Au_{36},[10] Au_{30},[11] Au_{28},[12] Au_{25},[13] Au_{24},[14] Au_{23},[15] and Au_{20}[16] were successfully determined by X-ray crystallography.

Recently, the mechanism of the formation of $[Au_{25}(SR)_{18}]$ nanoclusters has been studied,[17] in which the $[Au^I(SR)]$ complex is rapidly reduced to small Au nanoclusters, which have 2 or 4 free valence electrons (2e or 4e), and such small nanoclusters finally grow to the larger Au nanoclusters which have 8 free valence electrons. The $[Au_{15}(SR)_{13}]$ and $[Au_{18}(SR)_{14}]$ nanoclusters were found as the smallest gold–thiolate nanoclusters with 2 and 4 free valence electrons, respectively. Meanwhile, theoretical calculations also suggest that the most stable gold nanoclusters that have 2e and 4e are $[Au_{15}(SR)_{13}]$ and $[Au_{18}(SR)_{14}]$, respectively.[18] Thus, the $[Au_{15}(SR)_{13}]$ and $[Au_{18}(SR)_{14}]$ nanoclusters have a key role in the growth of gold nanoclusters. Unfortunately, no X-ray structure of them has been reported, only the DFT predicted structures.[18]

In this work, the Au_{18} nanocluster capped by L-glutathione (SG) is utilized as the starting material, which is subject to ligand exchange with cyclohexylthiol ($C_6H_{11}SH$). After changing the thiolate-ligands, the crystal structure of $[Au_{18}(SC_6H_{11})_{14}]$ could be determined. The Au_{18} nanocluster has an Au_9 core, which is constructed by two Au_6 cores. The Au_9 core is protected by three monomeric $Au(SR)_2$ staples, one dimeric $Au_2(SR)_3$ motif, and one tetrameric $Au_4(SR)_5$ motif. The dimeric and tetrameric of motifs cap the top and bottom of the Au_9 core, respectively. Meanwhile, one gold atom in this smallest of 4e nanoclusters belongs either to the core or the surface motif, it can thus be viewed as an "evolutionary" gold atom from Au^I to Au nanoclusters.

In a typical reaction, the $[Au_{18}(SC_6H_{11})_{14}]$ clusters were synthesized by a two-phase ligand-exchange approach, which involves two major steps: 1) synthesis of water-soluble $[Au_{18}(SG)_{14}]$ nanoclusters following the method reported by Pradeep et al.,[19] 2) two-phase ligand exchange, in which $[Au_{18}(SG)_{14}]$ nanoclusters were dissolved in water and then cyclohexylthiol dissolved in toluene (or CH_2Cl_2) was added to the cluster solution. A displacement kinetics experiment was carried out to track the reaction process (Supporting Information, Figure S1). The $[Au_{18}(SG)_{14}]$ nanoclusters were quickly deposited (Figure S1 and S2a), and the absorption ration (500 nm/600 nm, Figure S2c) did not change. Then the precipitate was dissolved in CH_2Cl_2 (Figure S1 and S2b), and the absorption ration (450 nm/524 nm or 450 nm/570 nm, Figure S2c) was quite steady. These results suggest that no by-product was obtained in water or in organic solvents systems. The differences in the UV/Vis absorption spectra of $[Au_{18}(SG)_{14}]$ (main peaks: 520 nm and 590 nm) and

[*] S. Chen,[+] S. Wang,[+] Y. Song, Dr. J. Zhang, Prof. H. Sheng, Prof. M. Zhu
Department of Chemistry and Centre for Atomic Engineering of Advanced Materials, Anhui University
Hefei, Anhui, 230601 (P.R. China)
E-mail: zmz@ahu.edu.cn
J. Zhong, Prof. Y. Pei
Department of Chemistry, Key Laboratory of Environmentally Friendly Chemistry and Applications of Ministry of Education, Xiangtan University
Hunan Province 411105 (P.R. China)
E-mail: ypnku78@gmail.com
[+] These authors contributed equally to this work.

[**] We acknowledge financial support by NSFC 21072001 & 21372006, the Ministry of Education and Ministry of Human Resources and Social Security, the Education Department of Anhui Province, Anhui Province International Scientific and Technological Cooperation Project, 211 Project of Anhui University. Y.P. is supported by NSFC (21103144, 21373176, 21422305), Hunan Provincial Natural Science Foundation of China (12JJ1003) and Scientific Research Fund of Hunan Provincial Education Department (13A100).

Supporting information for this article is available on the WWW under http://dx.doi.org/10.1002/anie.201410295.

$[Au_{18}(SR)_{14}]$ (main peaks: 570 nm and 640 nm) nanoclusters shows that the $[Au_{18}(SR)_{14}]$ nanocluster has an approximately 50 nm red shift. The red shift may be caused by ligand effect. The crystal structure of $[Au_{18}(SG)_{14}]$ was not obtain. The above results suggest that the cluster structure is unchanged by the ligand exchange. The IR spectrum was also used to monitor the water solution, the precipitate and the CH_2Cl_2 solution, respectively (Figure S3). A slightly enhanced ratio of Cy:SG (1923 cm^{-1}/1630 cm^{-1}, Figure S3a) was found in water soluble Au_{18} nanoclusters, indicating that the cyclohexythiol exchanged with the SG ligands in $[Au_{18}(SG)_{14}]$ nanoclusters, and this made the Au_{18} nanoclusters deposit quickly. The ratio of Cy:SG increased gradually in the precipitate (Figure S3b). When it was transferred to the organic solvent, no SG ligand was found in the organic-soluble Au_{18} nanoclusters (Figure S3c). HPLC separation further confirms our homogeneous preparation (Figure S4). The $[Au_{18}(SC_6H_{11})_{14}]$ nanoclusters exhibit weak photoluminescence centered at approximately 706 nm (see Figure S5) and the emission is weaker than that of 4e $[Au_{24}(SCH_2Ph\text{-}tBu)_{20}]$.[14] Using the well-studied $[Au_{25}(SG)_{18}]$ (where SG represent glutathione) as a reference (QY ≈ 0.2%), we found that the quantum yield of $[Au_{18}(SC_6H_{11})_{14}]$ is around 0.1%. The electrospray ionization mass spectrometry (ESI-MS) spectrum confirmed that the as-synthesized nanocluster retained its original size. We note that, without adding cesium acetate (CsOAc), no signal was found in either positive or negative mode, which implies charge neutrality of the cluster. To impart charges, the cluster solution was mixed with CsOAc to form positively charged $[M+Cs]^+$ adducts (where M represents the cluster) in the electrospray process. As shown in Figure 1A, the ESI-MS (positive ion mode) analysis revealed a prominent peak at *m/z* 5291.1, corresponding to the formula of the intact cluster $[Au_{18}(C_6H_{11}S)_{14}Cs]^+$ (calculated formula weight: 5291.1). Note that, the crude product has a similar ESI-MS spectrum (Figure S5) as that of the crystal sample, which indicates that the two-phase ligand exchange method can give rise to monodisperse nanoclusters.

The pure $[Au_{18}(SR)_{14}]$ nanoclusters were dissolved in CH_2Cl_2/MeCN (2:1), followed by slow diffusion of CH_2Cl_2 vapor into the cluster solution over a period of about 7 days at 18 °C. Dark green crystals were obtained, which were analyzed by single-crystal X-ray crystallography. The structure of $[Au_{18}(SR)_{14}]$ is shown in Figure 1B. The $[Au_{18}(SR)_{14}]$ structure has a Au_9 bi-octahedral kernel. This Au_9 core is built by two octahedral Au_6 units sharing one triangular face (Figure 1C). This Au_9^{5+} core is found for the first time in the Au nanoclusters, and it is larger than the Au_7 and Au_8 cores of $[Au_{20}(SR)_{16}]$ and $[Au_{24}(SR)_{20}]$, respectively. The octahedral Au_6 unit in this Au_9 core is a perfect fragment that can be cut out from face-centered-cubic (fcc) metals. Such an octahedral unit has also been identified in the Au_{28} and Au_{36} nanoclusters. The Au–Au distances in the Au_6 unit range from 2.6648(4) Å to 3.0068(5) Å (average 2.8262 Å), which is slightly shorter than the bulk gold Au–Au distance (2.88 Å). The Au_{core}–Au_{core} distance in the Au_{18} nanocluster is much longer than the $[Au_{20}(SR)_{16}]$ (average 2.72 Å) and $[Au_{24}(SR)_{20}]$(2.73 Å) nanoclusters.

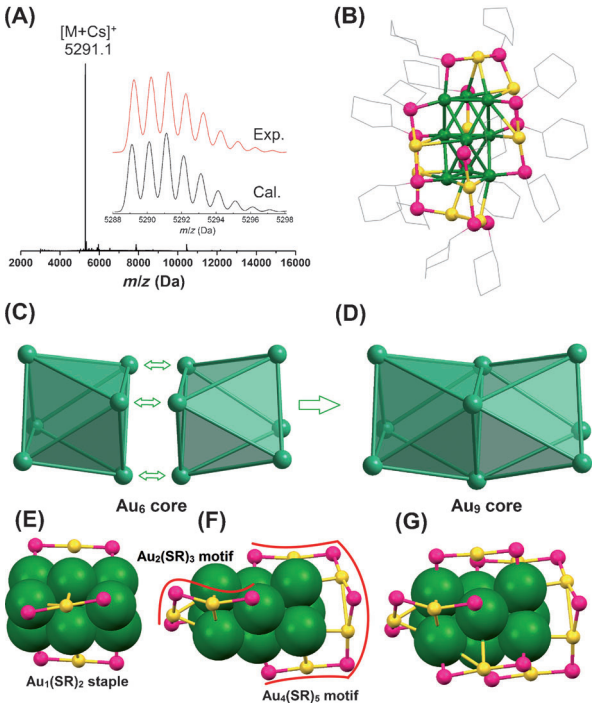

Figure 1. A) ESI-MS (positive ion mode) spectrum of $[Au_{18}(SC_6H_{11})_{14}]$ treated with CsOAc. Inset: experimental and simulated isotope patterns of $[Au_{18}(C_6H_{11}S)_{14}Cs]^+$. B) X-ray structure of $[Au_{18}(SC_6H_{11})_{14}]$; all hydrogen atoms are omitted for clarity. C) Anatomy of the Au_9 core as two Au_6 units; D) Bi-octahedral Au_9 kernel which is built by two octahedral Au_6 units sharing one triangular face. E) $Au(SR)_2$ staples protecting Au_9 kernel; F) dimeric and tetrameric staple motifs protecting Au_9 kernel; G) $[Au_{18}(SR)_{14}]$ structure. Dark green core Au, gold Au in the staple, red S.[25]

The bi-octahedral Au_9 kernel (Figure 1D) is protected by three monomeric staples (i.e., $Au(SR)_2$, Figure 1E), each S atom in these monomeric staples is linked to one Au atom at the end of the Au_9 core and one Au atom in the staple. In addition, one dimeric $Au_2(SR)_3$ and one tetrameric $Au_4(SR)_5$ motif (Figure 1F) are linked with the top and the bottom, forming the complete structure of the $[Au_{18}(SR)_{14}]$ nanocluster (Figure 1G). The strong interaction between the core and the ring, which is found in the $[Au_{20}(SR)_{16}]$ nanocluster, is also found in the $[Au_{18}(SR)_{14}]$ nanocluster structure. The gold–thiolate motif interacts with the core through Au_{motif}–Au_{core} bonds (3.09 ± 0.23 Å), which are quite strong as they are only 7.3% longer than the Au–Au distance of 2.88 Å in bulk gold.

The $[Au_{18}SR_{14}]$ nanocluster together with the previously reported $[Au_{20}(SR)_{16}]$ and $[Au_{24}(SR)_{20}]$ forms an "isoelectronic" 4e nanocluster family. The $[Au_{18}(SR)_{14}]$ nanocluster is the smallest member of these three nanoclusters, and is also predicted to be the smallest stable nanocluster with 4e electronic structure. More insights into the structure evolution from $Au^{I}SR$ complex to Au nanocluster can be gained by comparison with other 4e gold nanoclusters.

To study this evolution process, we focus on one special gold atom in the $[Au_{18}(SR)_{14}]$ nanocluster (Figure 2A, highlighted in black). This atom is linked to the four core atoms with average Au–Au distance of 2.786 Å and to two staple S

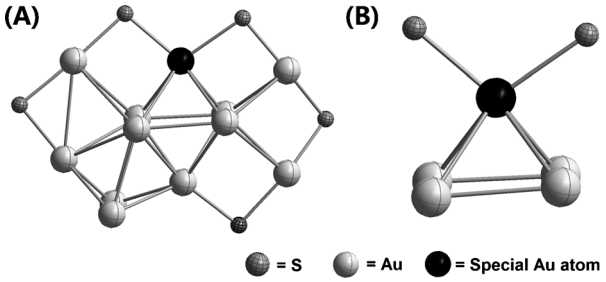

Figure 2. A) The special gold atom (black) which is linked with one $Au(SR)_2$ staple (left) and one $Au_2(SR)_3$ motif (right) and Au_6 core. B) Detailed view of (A) after removing the surrounding atoms.[25]

atoms with Au–S distances of 2.403/2.506 Å (Figure 2B). The special gold atom in $[Au_{18}(SR)_{14}]$ can be seen as a transitional $Au_4(SR)_5$ motif. This link mode was also found in $[Au_{102}(SR)_{44}]$ nanocluster. Generally, gold atoms can be classified as Au_{core} or Au_{motif}. In Au_{core}, Au is linked to at most one S atom, and the distance of Au_{core}–S is generally around 2.36 Å. In the Au_{motif} structure, every Au is linked with two S atoms. In both $[Au_{18}(SR)_{14}]$ and $[Au_{102}(SR)_{44}]$ nanoclusters, the distance between the special Au atom and the connected S atoms is much longer than other Au_{core}–S distance (ca + 8%). Xie et al. reported the growth mechanism of $[Au_{25}(SG)_{18}]$ nanoclusters, in which $[Au^I(SG)]$ complexes are first reduced to 2e $[Au_{15}(SG)_{13}]$ and 4e $[Au_{18}(SG)_{14}]$ nanoclusters, then grow to $[Au_{25}(SG)_{18}]$ nanoclusters.[17] On the basis of these results and the particular Au–S bonds found in the structure of $[Au_{18}(SR)_{14}]$ nanoclusters, we propose that, if the distance of the special Au and S in the $[Au_{18}(SR)_{14}]$ nanocluster is slightly lengthened, the Au–S bond will be broken, the gold atom will remain in the core, and the S atom will need another Au atom to form the Au–S staple. This may be the growth mechanism of the formation of larger gold nanoclusters.

To correlate the cluster structure and optical properties, we performed time-dependent density functional theory (TD-DFT) calculations for the electronic structure and optical absorption spectrum of $[Au_{18}(SR)_{14}]$ with $R = CH_3$ (see computational details in the Supporting Information. $R = C_6H_5$, C_6H_{11} were also calculated, see Figure S7). It can be found that the ligands do not significant affect the geometric structure of the AuS framework of $[Au_{18}(SR)_{14}]$. The calculated optical adsorption spectrum, energies, and atomic orbital (AO) component of Kohn–Sham molecular orbitals are displayed in Figure 3. As shown in Figure 3, the theoretical spectrum of $[Au_{18}(SCH_3)_{14}]$ shows feature peaks at 670 nm (peak a), 580 nm (peak b), 480 nm (peak c), and 380 nm (peak d), which qualitatively agree with the experimental results. Further examination of the Kohn–Sham (KS) molecular orbital (MO) energy levels and atomic orbital components in each KS MO of $[Au_{18}(SCH_3)_{14}]$ indicates that the occupied orbitals HOMO to HOMO−20 are mainly composed of the Au(5d) atomic orbitals, denoted as the d-band. The unoccupied orbitals are sp-band owing to the significant contribution of the Au(6sp) atomic orbitals. Because all the occupied orbitals are d-bands, the electronic transitions involved in all adsorption peaks are considered as

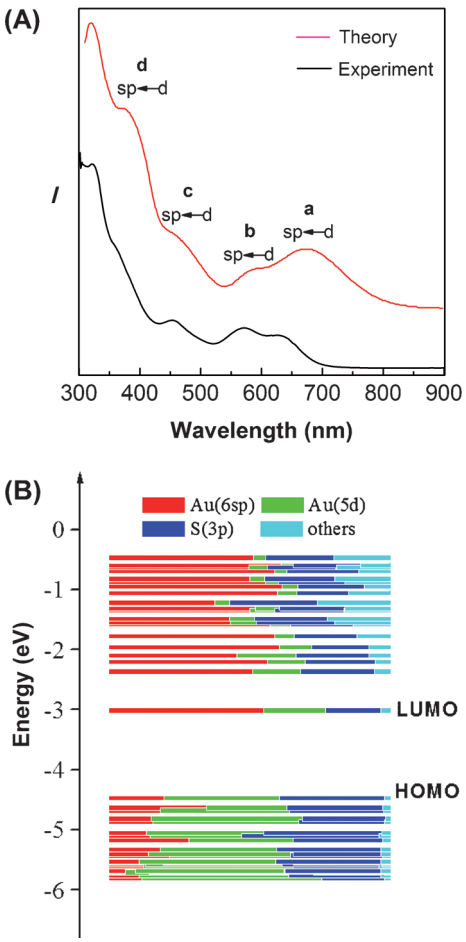

Figure 3. A) Simulated UV/Vis adsorption spectrum of $[Au_{18}(SR)_{14}]$. B) Kohn–Sham orbital energy level diagram for $[Au_{18}(SR)_{14}]$. The energies are in eV. Each Kohn–Sham orbital is drawn to indicate the relative contributions (line length with color labels) of the atomic orbitals of Au(6sp) red, Au(5d) green, S(3p) blue, and other orbital contributions from C and H atoms are in cyan.

d→sp interband transitions. We have also examined the components of KS orbitals and energy levels for $[Au_{24}(SCH_3)_{20}]$ and $[Au_{20}(SCH_3)_{16}]$, based on the recent reported crystal structures (Figure S8).[14,16] The computed diagram of KS orbital components indicate that the $[Au_{24}(SCH_3)_{20}]$ and $[Au_{20}(SCH_3)_{16}]$ have similar d→sp interband transitions to that of Au_{18} cluster, while larger $[Au_{25}(SR)_{18}]^-$ and $[Au_{38}(SR)_{24}]$ clusters with more free valence electronics are all have sp→sp interband transitions owing to the relatively larger contributions of the Au(6sp) atomic orbitals to HOMO.[13b,20]

The magic stability of $[Au_{18}(SR)_{14}]$ is further addressed in terms of superatom network (SAN) model[21] through analyzing the electronic structure of the Au core. The SAN model has been used to explain the magic stability of $[Au_{20}(SR)_{16}]$, $[Au_{28}(SR)_{20}]$, $[Au_{36}(SR)_{24}]$, and $[Au_{44}(SR)_{28}]$.[22] In these clusters, the Au^{z+} cores can be viewed as a network of tetrahedron Au_4-superatoms according to the SAN model. For example, the Au_{14}-core in $[Au_{28}(SR)_{20}]$ can be viewed as the fusion of four 2e superatom tetrahedral Au_4 units.

In the present case, the $[Au_{18}(SR)_{14}]$ is composed of a Au_9 core (protected by five staple motifs), which can be considered as Au_9^{5+} according to the superatom model.[23] The number of total valence electrons in Au_9^{5+} core is 4. In comparison to the Au core discovered in thiolated gold clusters, such as $[Au_{20}(SR)_{16}]$, $[Au_{25}(SR)_{18}]$, $[Au_{38}(SR)_{24}]$, $[Au_{28}(SR)_{20}]$, $[Au_{36}(SR)_{24}]$, and $[Au_{44}(SR)_{28}]$, the Au_9 core in $[Au_{18}(SR)_{14}]$ is composed of two fused octahedral Au_6 units, which suggests the 4e valence electrons might have a different distribution manner than in other gold clusters. To explore the distribution of the valence electrons, we performed chemical bond analysis of Au_9^{5+} using the adaptive natural density partitioning (AdNDP) method.[24] The AdNDP analysis is an efficient tool to explore the multi-centered bonds of atomic clusters by a scheme of orbital transformations. From Figure 4, two symmetric 6 center, 2 electron (6c-2e) bonds are clearly found within Au_9^{5+}, which both have occupancy numbers ON = 1.9897. The Au_9^{5+} can be therefore viewed as a unique combination of two fused superatom octahedral Au_6 units according to the SAN model.

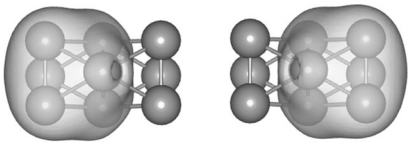

Figure 4. Two delocalized 6c-2e bonds from the AdNDP analysis of Au_9^{5+} core in $[Au_{18}(SR)_{14}]$. The ON denotes the occupation number of delocalized 6-center bond.

Another interesting finding is the boat form of cyclohexyl in the thiolate ligand. In the cyclohexylthiolate-protected $[Au_{18}(SR)_{14}]$ nanocluster, a boat-like form of cyclohexyl was found in the middle of the $Au_2(SR)_3$ motif (Figure S9). The ratio of boat/chair form is 1/13. Generally, the boat form of cyclohexyl is less stable than the chair form, and the ratio of boat/chair form of free cyclohexane is less than 0.1% at room temperature (significantly lower than the 7.7% percentage found in our $[Au_{18}(SC_6H_{11})_{14}]$ cluster structure). This phenomenon is not observed in the structure of cyclohexylthiolate-capped $[Au_{23}(SR)_{16}]^-$. The NMR spectrum of $[Au_{18}(SC_6H_{11})_{14}]$ was recorded in $CDCl_3$ solution (Figure S10), unfortunately, the core highly affects the ^1H shift of cyclohexyl and makes it hard to find the difference between the boat form and the chair form. It is plausible that the boat form cyclohexyl found in Au_{18} is due to the effect of the cluster core, but it might also be a solid-state effect caused by the consequence of crystal packing.

In summary, we have designed and synthesized cyclohexylthiolate ($C_6H_{11}S$) protected $[Au_{18}(SR)_{14}]$ nanoclusters by a ligand-exchange method and successfully solved the crystal structure. The $[Au_{18}(SR)_{14}]$ structure exhibits a new Au_9 bi-octahedral kernel, which is formed by two octahedral Au_6 units sharing one triangular face. Detailed analyses on the geometric and electronic structures offer insight into the evolution from $[Au^I(SR)]$ complex to Au nanoclusters. Future work on the smallest 2e $[Au_{15}(SR)_{13}]$ is expected to reveal more details of the $[Au^I(SR)]$ complex to Au nanocluster evolution process.[26]

Experimental Section

SG-caped Au_{18} nanoclusters were prepared by $NaBH_3CN$ reduction of $HAuCl_4$ in water in the presence of protonated L-glutathione (HSG).[18] The as-obtained $[Au_{18}(SG)_{14}]$ clusters were then used as the precursor for the synthesis of $[Au_{18}(SC_6H_{11})_{14}]$ by reaction with cyclohexylthiol. $[Au_{18}(SG)_{14}]$ (200 mg in 5 mL pure water) was added to a CH_2Cl_2 solution (5 mL) of cyclohexylthiol (1 mL) under vigorous stirring at 313 K. After 6 h, the product was transferred from water to CH_2Cl_2 solution, then the organic layer was separated and dried in vacuum, washed several times with ethanol/hexane (1:3, V/V). The pure $[Au_{18}(SR)_{14}]$ nanoclusters were then dissolved in CH_2Cl_2/MeCN (2:1), followed by slow vapor (CH_2Cl_2) diffusion into the cluster solution over about 7 days at 18 °C.

Received: October 21, 2014
Revised: December 7, 2014
Published online: January 23, 2015

Keywords: gold · nanoclusters · structure elucidation · sulfur ligands

[1] R. Jin, *Nanoscale* **2010**, *2*, 343 – 362.
[2] L. Gao, R. Jin, *Acc. Chem. Res.* **2013**, *46*, 1749 – 1758.
[3] G. Schmid, *Chem. Soc. Rev.* **2008**, *37*, 1909 – 1930.
[4] P. Maity, S. Xie, M. Yamauchi, T. Tsukuda, *Nanoscale* **2012**, *4*, 4027.
[5] J. Sun, Y. Jin, *J. Mater. Chem. C* **2014**, *2*, 8000 – 8011.
[6] a) R. Kubo, A. Kawabata, S. Kobayashi, *Annu. Rev. Mater. Sci.* **1984**, *14*, 49 – 66; b) Y. Negishi, K. Nobusada, T. Tsukuda, *J. Am. Chem. Soc.* **2005**, *127*, 5261 – 5270.
[7] a) J. W. A. van der Velden, F. A. Vollenbroek, J. J. Bour, P. T. Beurskens, J. M. M. Smits, W. P. Bosnian, *Recl. Trav. Chim. Pays-Bas* **1981**, *100*, 148 – 152; b) C. E. Briant, K. P. Hall, D. M. P. Mingos, A. C. Wheeler, *J. Chem. Soc. Dalton Trans.* **1986**, 687 – 692; c) J. W. A. Van der Velden, J. J. Bour, J. J. Steggerda, P. T. Beurskens, M. Roseboom, J. H. Noordik, *Inorg. Chem.* **1982**, *21*, 4321 – 4324; d) Y. Shichibu, M. Zhang, Y. Kamei, K. Konishi, *J. Am. Chem. Soc.* **2014**, *136*, 12892 – 12895; e) Y. Kamei, Y. Shichibu, K. Konishi, *Angew. Chem. Int. Ed.* **2011**, *50*, 7442 – 7445; *Angew. Chem.* **2011**, *123*, 7580 – 7583; f) N. Kobayashi, Y. Kamei, Y. Shichibu, K. Konishi, *J. Am. Chem. Soc.* **2013**, *135*, 16078 – 16081; g) A. Purath, R. Köppe, H. Schnökel, *Chem. Commun.* **1999**, 1933 – 1934.
[8] P. D. Jadzinsky, G. Calero, C. J. Ackerson, D. A. Bushnell, R. D. Kornberg, *Science* **2007**, *318*, 430 – 433.
[9] H. Qian, W. T. Eckenhoff, Y. Zhu, T. Pintauer, R. Jin, *J. Am. Chem. Soc.* **2010**, *132*, 8280 – 8281.
[10] a) C. Zeng, H. Qian, T. Li, G. Li, N. L. Rosi, B. Yoon, R. N. Barnett, R. L. Whetten, U. Landman, R. Jin, *Angew. Chem. Int. Ed.* **2012**, *51*, 13114 – 13118; *Angew. Chem.* **2012**, *124*, 13291 – 13295; b) A. Das, C. Liu, C. Zheng, G. Li, T. Li, N. L. Rosi, R. Jin, *J. Phys. Chem. A* **2014**, *118*, 8264 – 8269.
[11] a) D. Crasto, S. Malola, G. Brosofsky, A. Dass, H. Häkkinen, *J. Am. Chem. Soc.* **2014**, *136*, 5000 – 5005; b) H. Yang, Y. Wang, A. J. Edwards, J. Yan, N. Zheng, *Chem. Commun.* **2014**, *50*, 14325 – 14327.
[12] C. Zeng, T. Li, A. Das, N. L. Rosi, R. Jin, *J. Am. Chem. Soc.* **2013**, *135*, 10011 – 10013.
[13] a) M. W. Heaven, A. Dass, P. S. White, K. M. Holt, R. W. Murray, *J. Am. Chem. Soc.* **2008**, *130*, 3754 – 3755; b) M. Zhu,

C. M. Aikens, F. J. Hollander, G. C. Schatz, R. Jin, *J. Am. Chem. Soc.* **2008**, *130*, 5883 – 5885; c) M. Zhu, W. T. Eckenhoff, T. Pintauer, R. Jin, *J. Phys. Chem. C* **2008**, *112*, 14221 – 14224.
[14] A. Das, T. Li, G. Li, K. Nobusada, C. Zeng, N. L. Rosi, R. Jin, *Nanoscale* **2014**, *6*, 6458 – 6462.
[15] A. Das, T. Li, K. Nobusada, C. Zeng, N. L. Rosi, R. Jin, *J. Am. Chem. Soc.* **2013**, *135*, 18264.
[16] C. Zeng, C. Liu, Y. Chen, N. L. Rosi, R. Jin, *J. Am. Chem. Soc.* **2014**, *136*, 11922 – 11925.
[17] Z. Luo, V. Nachammai, B. Zhang, N. Yan, D. T. Leong, D. Jiang, J. Xie, *J. Am. Chem. Soc.* **2014**, *136*, 10577 – 10580.
[18] a) A. Tlahuice, I. L. Garzon, *Phys. Chem. Chem. Phys.* **2012**, *14*, 3737 – 3740; b) D. Jiang, S. H. Overbury, S. Dai, *J. Am. Chem. Soc.* **2013**, *135*, 8786 – 8789; c) A. Tlahuice-Flores, M. Jose-Yacaman, R. L. Whetten, *Phys. Chem. Chem. Phys.* **2013**, *15*, 19557 – 19560.
[19] A. Ghosh, T. Udayabhaskararao, T. Pradeep, *J. Phys. Chem. Lett.* **2012**, *3*, 1997 – 2002.
[20] Y. Pei, Y. Gao, X. C. Zeng, *J. Am. Chem. Soc.* **2008**, *130*, 7830 – 7832.
[21] a) L. Cheng, Y. Yuan, X. Zhang, J. Yang, *Angew. Chem. Int. Ed.* **2013**, *52*, 9035 – 9039; *Angew. Chem.* **2013**, *125*, 9205 – 9209; b) L. Cheng, C. Ren, X. Zhang, J. Yang, *Nanoscale* **2013**, *5*, 1475 – 1478.
[22] Y. Pei, S. Lin, J. Su, C. Liu, *J. Am. Chem. Soc.* **2013**, *135*, 19060 – 19063.
[23] M. Walter, J. Akola, O. Lopez-Acevedo, P. D. Jadzinsky, G. Calero, C. J. Ackerson, R. L. Whetten, H. Grönbeck, H. Häkkinen, *Proc. Natl. Acad. Sci. USA* **2008**, *105*, 9157.
[24] a) Y. D. Zubarev, A. I. Boldyrev, *Phys. Chem. Chem. Phys.* **2008**, *10*, 5207 – 5217; b) T. Lu, F. Chen, *J. Comput. Chem.* **2012**, *33*, 580 – 592; c) D. Y. Zubarev, A. I. Boldyrev, *J. Phys. Chem. A* **2009**, *113*, 866 – 868.
[25] CCDC 104485 contains the supplementary crystallographic data for this paper. These data can be obtained free of charge from The Cambridge Crystallographic Data Centre via www.ccdc.cam.ac.uk/data_request/cif.
[26] After acceptance of this manuscript we learnt of another publication reporting the crystal structure of a $[Au_{18}(SR)_{14}]$ nanocluster: A. Das, C. Liu, H. Y. Byun, K. Nobusada, S Zhao, N. L. Rosi, R. Jin, *Angew. Chem. Int. Ed.* **2015**, DOI: 10.1002/anie.201410161; *Angew. Chem.* **2015**, DOI: 10.1002/ange.201410161.

